Journal of Hazardous Materials 457 (2023) 131800

Contents lists available at ScienceDirect

Journal of Hazardous Materials

journal homepage: www.elsevier.com/locate/jhazmat

Research Paper

Tuning the intrinsic catalytic sites of magnetite to concurrently enhance the reduction of H_2O_2 and O_2: Mechanism analysis and application potential evaluation

Ling Li [a], Min Cheng [a], Eydhah Almatrafi [b], Lei Qin [a], Shiyu Liu [a], Huan Yi [a], Lu Yang [a], Zhexin Chen [a], Dengsheng Ma [a], Mingming Zhang [a], Xuerong Zhou [a], Fuhang Xu [a], Chengyun Zhou [a,b], Lin Tang [a], Guangming Zeng [a,b,*], Cui Lai [a,**]

[a] College of Environmental Science and Engineering and Key Laboratory of Environmental Biology and Pollution Control (Ministry of Education), Hunan University, Changsha 410082, PR China

[b] Center of Research Excellence in Renewable Energy and Power Systems, Center of Excellence in Desalination Technology, Department of Mechanical Engineering, Faculty of Engineering-Rabigh, King Abdulaziz University, Jeddah 21589, Saudi Arabia

HIGHLIGHTS

- A facile strategy was examined to synthesize Fe_3O_4 with oxygen vacancies.
- H_2O_2 tended to lose e^- on Fe sites of Fe_3O_4 and gain e^- on OVs sites of V_o-Fe_3O_4.
- The OVs sites promoted dissolved oxygen activation and conversion of $O_2^{\bullet-}$ to $^1O_2$.
- V_o-Fe_3O_4/H_2O_2 system performed well in both batch and continuous-flow reactor.

GRAPHICAL ABSTRACT

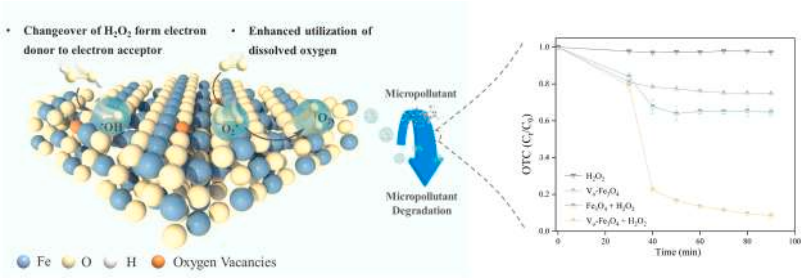

ARTICLE INFO

Editor: Sungjun Bae

Keywords:
Fe_3O_4
Oxygen vacancies
H_2O_2 activation
Electron transfer
Water treatment

ABSTRACT

Heterogeneous Fenton-like process based on H_2O_2 activation has been widely tested for water purification, but its application still faces some challenges such as the use of high doses of chemicals (including catalysts and H_2O_2). Herein, a facile co-precipitation method was utilized for small-scale production (~50 g) of oxygen vacancies (OVs)-containing Fe_3O_4 (V_o-Fe_3O_4) for H_2O_2 activation. Experimental and theoretical results collaboratively verified that H_2O_2 adsorbed on the Fe site of Fe_3O_4 tended to lose electrons and generate $O_2^{\bullet-}$. While the localized electron from OVs of V_o-Fe_3O_4 could assist in donating electrons to H_2O_2 adsorbed on OVs sites, this allowed more H_2O_2 to be activated to $^{\bullet}OH$, which was 3.5 folds higher than Fe_3O_4/H_2O_2 system. Moreover, the OVs sites promoted dissolved oxygen activation and decreased the quenching of $O_2^{\bullet-}$ by Fe(III), thus promoting the generation of $^1O_2$. Consequently, the fabricated V_o-Fe_3O_4 achieved much higher oxytetracycline (OTC) degradation rate (91.6%) than Fe_3O_4 (35.4%) at a low catalyst (50 mg/L) and H_2O_2 dosage (2 mmol/L). Importantly, further integration of V_o-Fe_3O_4 into fixed-bed Fenton-like reactor could effectively eliminate OTC

* Corresponding author at: College of Environmental Science and Engineering and Key Laboratory of Environmental Biology and Pollution Control (Ministry of Education), Hunan University, Changsha 410082, PR China.
** Corresponding author.
E-mail addresses: zgming@hnu.edu.cn (G. Zeng), laicui@hnu.edu.cn (C. Lai).

https://doi.org/10.1016/j.jhazmat.2023.131800
Received 5 April 2023; Received in revised form 22 May 2023; Accepted 6 June 2023
Available online 7 June 2023

(>80%) and chemical oxygen demand (COD) (21.3%~50%) within the running period. This study provides promising strategies for enhancing the H_2O_2 utilization of Fe mineral.

1. Introduction

Owing to their abundance in Earth's crust, environment-friendly performance, and capacity of activating hydrogen peroxide (H_2O_2), iron-based minerals, such as goethite (FeOOH), hematite (Fe_2O_3) and magnetite (Fe_3O_4) have aroused interesting attention in heterogeneous Fenton-like reaction for treating polluted wastewater in recent years [1–4]. Thereinto, Fe_3O_4 may be more attractive owing to the presence of intrinsic Fe(II) for H_2O_2 activation and superior magnetic properties for separation [5,6]. Nevertheless, the H_2O_2 utilization efficiency of Fe_3O_4 is usually very low on account of the aggregation of Fe_3O_4 and insufficient iron cycle (Fe(III)/Fe(II)) during Fenton-like reaction [3,7]. As described in previous literature, excessive doses of H_2O_2 (10–50 mmol/L) was typical required to degrade relatively low concentrations of organic pollutants (0.01–0.3 mmol/L) in Fe_3O_4-based heterogeneous Fenton-like system (Table S1) [8–14]. The attempt to reduce H_2O_2 consumption is thus of great significance.

Such an objective can be achieved by tuning the intrinsic catalytic sites of Fe_3O_4 to modulate its Fenton-like activity [15,16]. In fact, except for the traditional surface Fe sites of Fe oxides, some microstructures over Fe oxides, such as oxygen vacancies (OVs) and electron distribution-polarized micro-areas have also been investigated as potential catalytic sites for H_2O_2 activation in recent years [17–20]. Taken OVs as example, it has been reported that OVs are possible to modify the surface electronic structure of metal oxides and enhance their electronic conductivity, thus positively affecting the metal redox cycle and interfacial electron transfer between metal oxides and H_2O_2 [21,22]. On the other hand, OVs may act as reactive sites for substrates (i.e., H_2O_2 and dissolved oxygen (DO)) adsorption as well as activation due to the coordinative unsaturation property and accumulated local electrons, then accelerating the production of reactive species [23,24]. Our previous work also reported that the existence of OVs prominently altered the surface properties of CuO, and switched the reaction mechanism from •OH generation to the major formation of Cu(III) [25].

Inspired by the above processes, it can be envisaged that preparing Fe_3O_4 with dual-catalytic sites through modulating OVs should be a promising strategy to enhance the H_2O_2 utilization efficiency and catalytic performance. Nevertheless, to date, scale production of OVs-containing Fe_3O_4 (V_o-Fe_3O_4) in a facile method is still challenging. Moreover, the following concerns, including (i) the electron transfer process between H_2O_2 and V_o-Fe_3O_4; (ii) the influence of synergistic effects between OVs and surface Fe sites on reactive species generation; and (iii) the scale-up application performance of the obtained catalyst, remain to be unrevealed, which still needs to be further investigated for promoting the practical application.

Therefore, in this study, a convenient and eco-friendly coprecipitation method is employed to prepare OVs-rich Fe_3O_4 (V_o-Fe_3O_4). Then, the Fenton-like activity of the obtained catalyst is studied by degrading oxytetracycline (OTC), a typically antibiotic in water environment, in batch reactor and continuous fixed-bed reactor. Other characteristics during Fenton-like reaction such as (i) the utilization efficiency of H_2O_2; (ii) the influence of experimental conditions including H_2O_2 dosage, initial pH and co-existing anions on catalytic performance are discussed. Besides, the interfacial reactions between V_o-Fe_3O_4 and H_2O_2, as well as the generation mechanism of reactive species are explored in depth by combining experimental and theoretical studies.

2. Materials and methods

2.1. Materials

Ammonium hydroxide ($NH_3{\cdot}H_2O$), H_2O_2, sodium borohydride ($NaBH_4$), ferrous sulfate heptahydrate ($FeSO_4{\cdot}7\ H_2O$), ferric chloride hexahydrate ($FeCl_3{\cdot}6\ H_2O$), OTC, 2,2,6,6-tetramethylpiperidine (TEMPOL), tert-butyl alcohol (TBA), L-tryptophan, 1,3-diphenylisobenzofuran (DPBF), sodium hydroxide (NaOH), hydrogen chloride (HCl), and quartz sand were purchased from Sinopharm Chemical Reagent Corp (Beijing, China). Ultrapure water, of which the resistivity was 18.25 MΩ•cm, was applied throughout the experiment.

2.2. Preparation of catalysts

Fe_3O_4 was synthesized through co-precipitation method. To be specific, 0.02 mol $FeSO_4{\cdot}7\ H_2O$ and 0.04 mol $FeCl_3{\cdot}6\ H_2O$ were dissolved in oxygen-free water (40 mL) to obtain a mixed solution. Subsequently, $NH_3{\cdot}H_2O$ (12 mL) was added dropwise at 80 °C and stirred for 5 min, the obtained suspension was named as A. Then, 12 mL oxygen-free water was added dropwise into A and further stirred for 2 h. The obtained black solid was filtered and washed with ultrapure water and ethanol several times to acquire Fe_3O_4. For synthesizing V_o-Fe_3O_4, 12 mL $NaBH_4$ ($C_{(NaBH4)}$ = 2 mol/L) instead of oxygen-free water was added drop-wise into A, and the rest of steps were the same as Fe_3O_4 synthesis. For scale production of V_o-Fe_3O_4, 0.3 mol $FeSO_4{\cdot}7\ H_2O$ and 0.6 mol $FeCl_3{\cdot}6\ H_2O$ were dissolved in 600 mL oxygen-free water to obtain a mixed solution. The following steps were the same as V_o-Fe_3O_4 synthesis, and the volume of $NH_3{\cdot}H_2O$ as well as $NaBH_4$ ($C_{(NaBH4)}$ = 2 mol/L) was 180 mL.

2.3. Characterization of catalysts

A detailed description of the characterization technologies and methods of density functional theory (DFT) calculations [26–34] is included in Text S1.

2.4. Experimental procedure

2.4.1. Stirred reactor experiment

Firstly, OTC solution (10 mg/L) was prepared in a volume of 100 mL. Then 5 mg of catalyst was added into the solution, and adsorption/desorption equilibrium was acquired by stirring for 30 min. For triggering Fenton-like reaction, H_2O_2 (1 mol/L) was then added. Besides, samples were taken out during each interval, filtrated through a 0.22 μm Millipore membrane filter, and then quenched by adding 70 μL of TBA. The above solution was used for analysis. For studying the effect of solution pH on Fenton-like activity, the solution pH was adjusted by NaOH and HCl. For studying the performance of V_o-Fe_3O_4 in natural water, OTC solution (10 mg/L) was prepared by using lake water (Taozi Lake, Changsha, China) and river water (Xiangjiang River, Changsha, China) as solvent.

2.4.2. Fixed-bed reactor experiments

For fixed-bed reactor experiments, four parts including wastewater storage (containing OTC and H_2O_2), peristaltic pump, packed bed (including 0.05 g of catalyst and 50 g of quartz sand), and fraction collector were involved. The whole reaction was propelled by the power provided by the peristaltic pump. Meanwhile, 5 mL of the sample was collected at regular intervals for further analysis.

2.5. Analytical methods

The residual OTC concentration was determined through high performance liquid chromatography (HPLC, Agilent 1260, USA), where the mobile phase consisted of methanol, acetonitrile, and 0.005 mol/L oxalic acid (15: 10: 75 (v/v/v)), the flow rate was 1 mL/min, and detection wavelength was 355 nm. Besides, Shimadzu TOC-VCPH analyzer was applied to study the total organic carbon (TOC) removal efficiency. HACH DR/2010 spectrophotometer was used to measure the chemical oxygen demand (COD) value. The leaching amount of Fe during reaction was detected by inductively coupled plasma mass spectrometry (ICP-MS, Agilent 7900). High-performance liquid chromatography-mass spectrometry (HPLC-MS, 1290/6460 Triple Quad) was employed for studying the degradation intermediates of OTC.

The variation of H_2O_2 concentration during Fenton-like process was detected by a titanium (IV) (Ti(IV)) colorimetric method [35]. In-situ detection of superoxide radical ($O_2^{\bullet-}$), hydroxyl radical ($^{\bullet}OH$), and singlet oxygen ($^1O_2$) was performed through electron paramagnetic resonance (EPR) technology (Bruker EMXplus spectrometer), where DMPO and TEMP were used as spin-trap reagents, respectively. Quantification of $^{\bullet}OH$ was conducted by employing 2 mmol/L benzoic acid (BA) as a probe. It was known that BA reacting with 5.87 ± 0.18 moles •OH produced one mole p-hydroxybenzoic acid (p-HBA) [36], the generated p-HBA could then be detected by HPLC. The mobile phase consisted of 0.1% acetic acid and methanol (50: 50 (v/v)) with detection wavelength to be 254 nm.

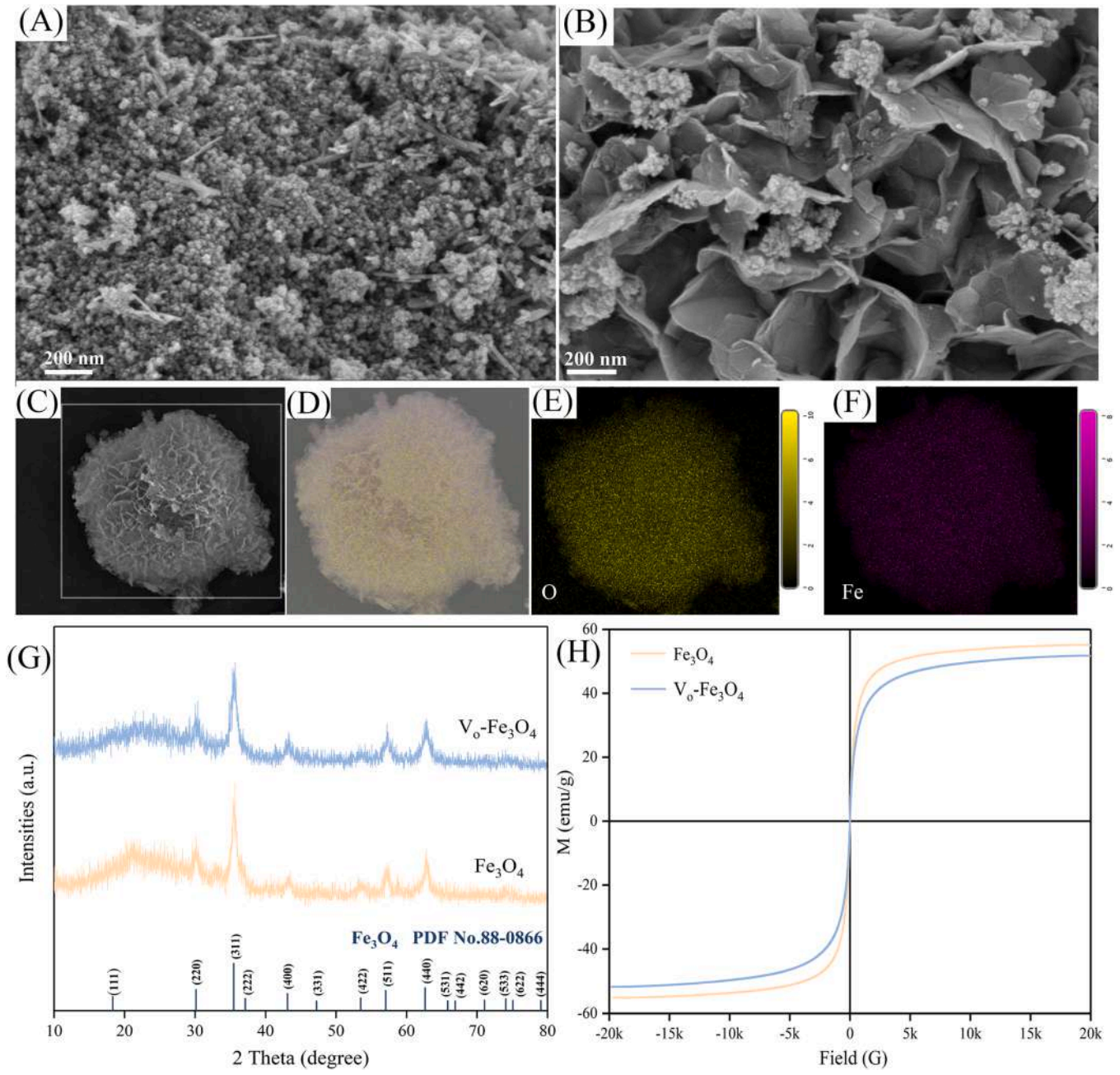

Fig. 1. SEM images of (A) Fe_3O_4, and (B-C) V_o-Fe_3O_4; (D-F) EDS-elemental manning of V_o-Fe_3O_4; (G) XRD patterns, and (H) magnetic hysteresis loops of Fe_3O_4 and V_o-Fe_3O_4.

3. Results and discussion

3.1. Characterization of catalysts

Fig. 1(A-C) shows the scanning electron microscope (SEM) images of obtained materials. As displayed in Fig. 1 (A), Fe_3O_4 mainly existed in spherical morphologies with partial in rod-like morphologies. Meanwhile, it was found that V_o-Fe_3O_4 exhibited a flower-like nanostructure constructed by several nanosheets (Fig. 1(B-C)). These results indicated that treating Fe_3O_4 precursor with $NaBH_4$ had significant influence on the morphology, this was probably because the addition of $NaBH_4$ affected the nucleation and aggregation growth rate of Fe_3O_4 precursor [37,38]. In addition, the elemental composition of V_o-Fe_3O_4 was further studied by energy-dispersive spectrometry (EDS)-elemental mapping (Fig. 1(D-F)), which suggested the uniform distribution of Fe and O.

The X-ray diffractometer (XRD) patterns of obtained catalysts are presented in Fig. 1(G). As can be seen, both Fe_3O_4 and V_o-Fe_3O_4 showed characteristic diffraction peaks at 2θ around 30.1°, 35.5°, 43.1°, 53.5°, 57.0°, and 62.6°, belonging to the (220), (311), (400), (422), (511), and (440) crystal planes of Fe_3O_4, respectively (PDF No.88–0866) [8]. Meanwhile, the clear lattice fringes were observed from the high-resolution transmission electron microscope (HRTEM) images of V_o-Fe_3O_4 (Fig. S1), and the lattice spacing was about 0.219 nm, 0.254 nm and 0.298 nm, corresponding to the (400), (311) and (220) facets of Fe_3O_4, respectively. This further verified that the structure of V_o-Fe_3O_4 belonged to Fe_3O_4.

The magnetization properties of obtained catalysts were then studied by vibrating sample magnetometer (VSM). It can be found from magnetic hysteresis loops (Fig. 1(H)) that both Fe_3O_4 and V_o-Fe_3O_4 exhibited strong magnetic response to the changed magnetic fields (Table 1). Meanwhile, the saturated magnetization (Ms) of V_o-Fe_3O_4 was slightly lower than that of Fe_3O_4, and this may be due to the magnetocrystalline anisotropy of Fe_3O_4. As previously reported, the magnetic properties of Fe_3O_4 showed anisotropy along the axis of the crystal, and in this case, Fe_3O_4 with different morphological structures might exhibit different magnetic properties [9].

Besides, the pore characteristic and surface area of Fe_3O_4 and V_o-Fe_3O_4 were explored via N_2 adsorption-desorption isotherms. The results are presented in Fig. S2 and Table 1. It can be observed that the BET specific surface area of V_o-Fe_3O_4 increased compared to Fe_3O_4, which may be due to the flower-like structure of V_o-Fe_3O_4 alleviating the aggregation of nanoparticles, and therefore enlarging the specific surface area. Generally, a larger surface area may allow the catalyst to expose more reactive sites for substrate contact, which then favors the catalytic process.

Additionally, the surface chemical states of catalysts were studied via X-ray photoelectron spectroscopy (XPS). The XPS survey demonstrated the existence of O and Fe in the obtained materials (Fig. 2(A)). Besides, O 1 s spectra of Fe_3O_4 (Fig. 2(B)) could be deconvoluted into three peaks, including O-H from surface-absorbed water (O_{OH} at 533.3 eV), oxygen species chemisorbed at OVs sites (O_V at 531.4 eV), and lattice oxygen (O_L at 530.1 eV) [18,39,40]. The area of O_V was higher for V_o-Fe_3O_4 (Fig. 2(C)) than Fe_3O_4, suggesting that V_o-Fe_3O_4 possessed more OVs among these two samples. The high-resolution XPS spectra of Fe 2p further confirmed this statement. As displayed in Fig. 2(D), the peaks at 711.1 eV and 724.7 eV could be attributed to the Fe $2p_{3/2}$ and Fe $2p_{1/2}$ of Fe(II) oxidation state, respectively [41,42]. Meanwhile, the binding energies of the other two peaks were 713.1 eV and 727.1 eV, respectively, which belonged to Fe(III) [43]. Compared with Fe_3O_4, the peak area ratio of Fe(II) to Fe(III) in V_o-Fe_3O_4 increased. This might be because the electrons around OVs could be easily attracted by neighboring metal ions and then led to the reduction of metal ions [18].

The existence of OVs was further confirmed by EPR technology (Fig. 2(F)). It can be observed that both Fe_3O_4 and V_o-Fe_3O_4 showed signal with g value of 2.003, which was the typical signal example of OVs [39,44]. Meanwhile, V_o-Fe_3O_4 exhibited stronger intensity among these samples, further verifying that a higher concentration of OVs was obtained in V_o-Fe_3O_4. As reported by some literatures, the oxidation state of metal ions would be decreased when metal oxide underwent redox reaction with $NaBH_4$, which would result in the generation of OVs (anion defects) because of the charge neutrality of crystal [18,45]. To further reveal the effect of OVs on electronic structure of Fe_3O_4, the charge density difference before and after introduction of OVs was investigated by DFT calculation. As observed from Fig. 3(C-D), the electron density of Fe atom increased with the introduction of OVs, suggesting the enhancement of Fe reduction, which was consistent with the XPS results.

Table 1
BET specific surface area, pore diameter, pore volume, saturated magnetization (Ms), and remnant magnetization (Mr) of obtained catalysts.

Samples	Fe_3O_4	V_o-Fe_3O_4
BET specific Surface area (m^2/g)	98.07	113.48
Pore volume (cm^3/g)	0.33	0.31
Pore diameter (nm)	11.87	10.09
Ms (emu g^{-1})	55.03	51.72
Mr (emu g^{-1})	1.15	0.46

3.2. Catalytic performance in bacth reactor

Then, the Fenton-like activities of Fe_3O_4 and V_o-Fe_3O_4 were evaluated by studying the results of OTC degradation. Obviously, OTC concentration barely decreased in the presence of H_2O_2 alone (Fig. 4(A)), suggesting that H_2O_2 could hardly degrade OTC. Meanwhile, OTC concentration decreased by about 35.4% in Fe_3O_4/H_2O_2 system. In contrast, 91.6% of OTC could be degraded in V_o-Fe_3O_4/H_2O_2 system, and only 25.2% of OTC can be removed when using V_o-Fe_3O_4 alone, indicating that the interaction between V_o-Fe_3O_4 and H_2O_2 played an important role in OTC degradation. In addition, the pseudo-first-order kinetic for OTC degradation was also studied. It could be found from Fig. 4(B) that the rate constant of V_o-Fe_3O_4/H_2O_2 system was 0.0311 min^{-1}, which was about 10 times higher than that of Fe_3O_4/H_2O_2 system (k = 0.003 min^{-1}).

In order to further study the Fenton-like activity of Fe_3O_4 and V_o-Fe_3O_4 during reaction, the utilization rate of H_2O_2 (η) was calculated based on the previous described method (Text S2) [46,47]. In general, H_2O_2 utilization efficiency is defined as the ratio of stoichiometric H_2O_2 consumption ($[\triangle H_2O_2]_S$) for pollutants mineralization to the actual H_2O_2 consumption ($[\triangle H_2O_2]_A$). As shown in Fig. 4(C), the $[\triangle H_2O_2]_A$ for Fe_3O_4 and V_o-Fe_3O_4 within 90 min was 0.08 mmol/L and 0.65 mmol/L, and TOC removal efficiency was determined to be 4.1% and 39.2%, respectively (Fig. S3). Then, the H_2O_2 utilization efficiency by different catalysts was calculated and ordered as V_o-Fe_3O_4 (62.8%)> Fe_3O_4 (52.5%) (Table S2). Thus, it can be concluded that V_o-Fe_3O_4 showed higher Fenton-like activity, which may be because: (i) the flower-like nanostructure and increased surface area facilitated the exposure of reactive sites for OTC and H_2O_2 contact; (ii) the existence of more OVs could promote Fe(II) generation and act as reactive site (see Section 3.4 for detail), therefore enhancing H_2O_2 activation; and (iii) the generated OVs could enhance the electronic conductivity of catalyst and accelerate the electron transfer. This was confirmed by the liner sweep voltammetry (LSV) results (Fig. 4(D)), where the current response in V_o-Fe_3O_4/H_2O_2 system was stronger than that in Fe_3O_4/H_2O_2 system, indicating the accelerated electron transfer process in V_o-Fe_3O_4/H_2O_2 system. Electrochemical impedance spectroscopy (EIS) results also supported this statement (Fig. 4(D)), in which V_o-Fe_3O_4 exhibited a smaller semicircle diameter than Fe_3O_4, indicating its lower interfacial charge transfer resistance.

3.2.1. Effect of operating factors

As for the effect of H_2O_2 dosage, it was found that OTC degradation

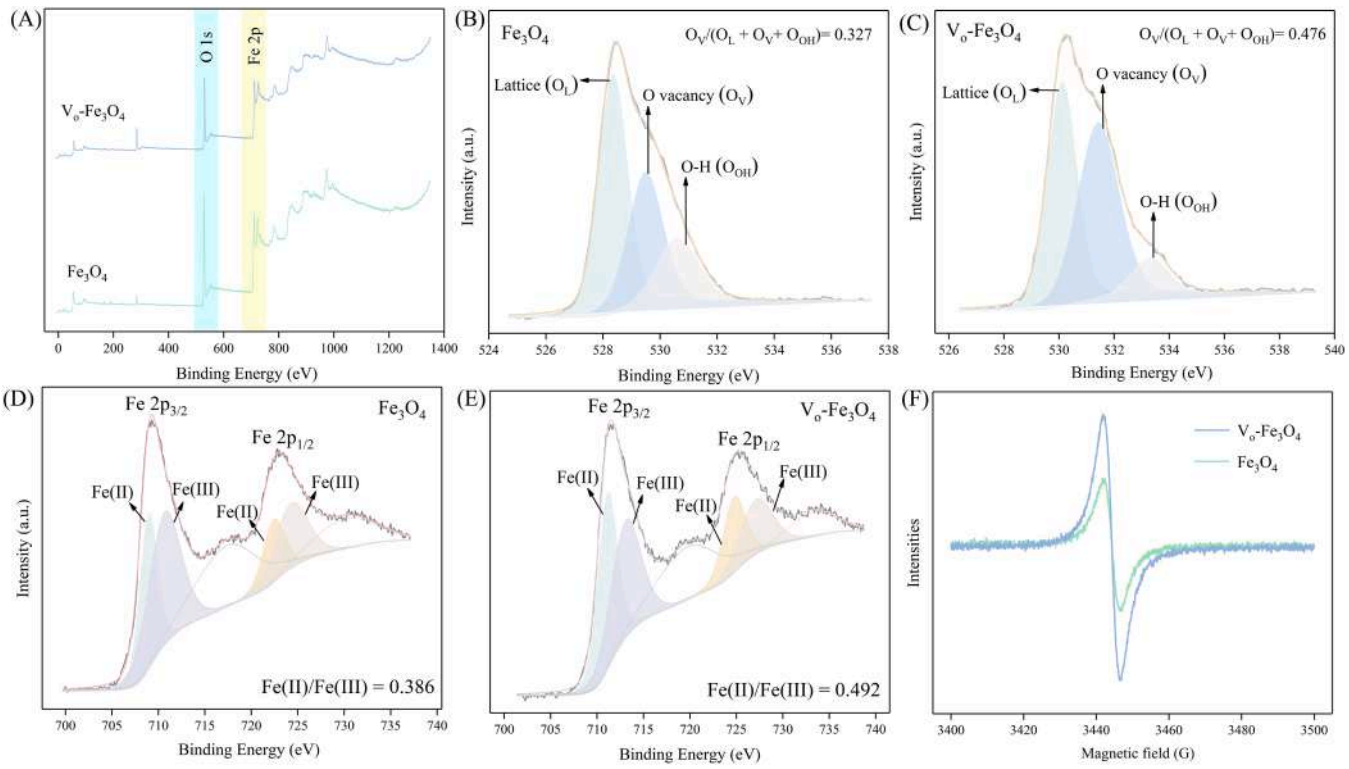

Fig. 2. (A) XPS survey of Fe_3O_4 and V_o-Fe_3O_4; O 1 s spectra of (B) Fe_3O_4 and (C) V_o-Fe_3O_4; Fe 2p spectra of (D) Fe_3O_4 and (E) V_o-Fe_3O_4; (F) EPR spectra of Fe_3O_4 and V_o-Fe_3O_4.

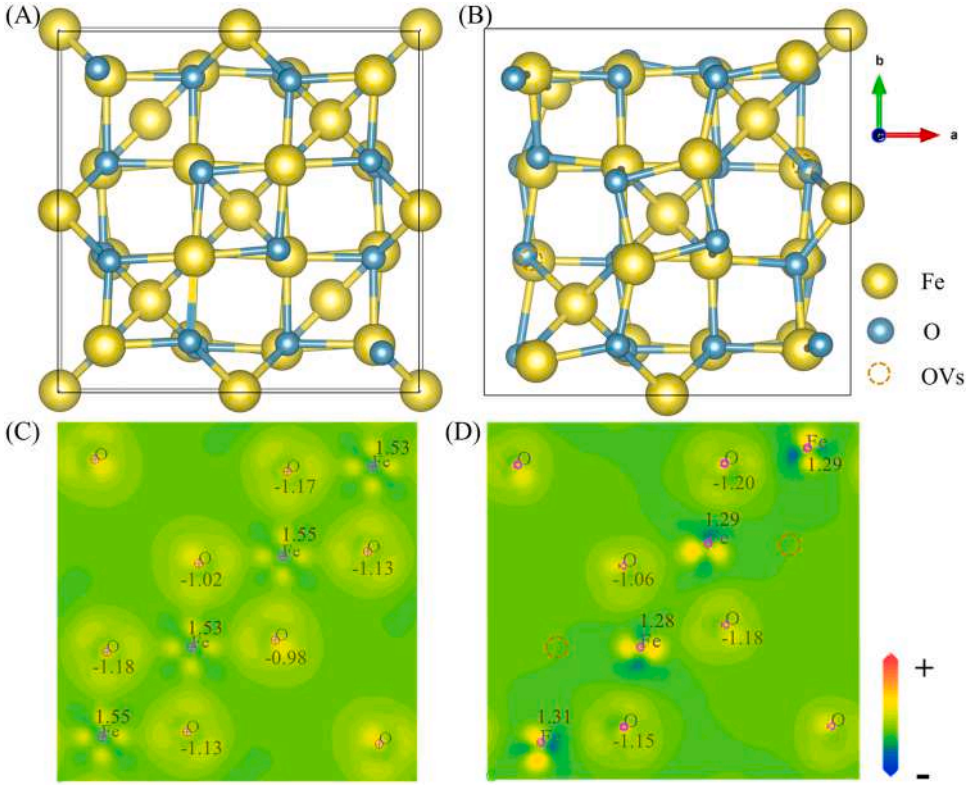

Fig. 3. Top view structures of (A) Fe_3O_4 (001) plane and (B) V_o-Fe_3O_4 (001) plane; Slices of top view charge density difference of (C) Fe_3O_4 (001) plane and (D) V_o-Fe_3O_4 (001) plane.

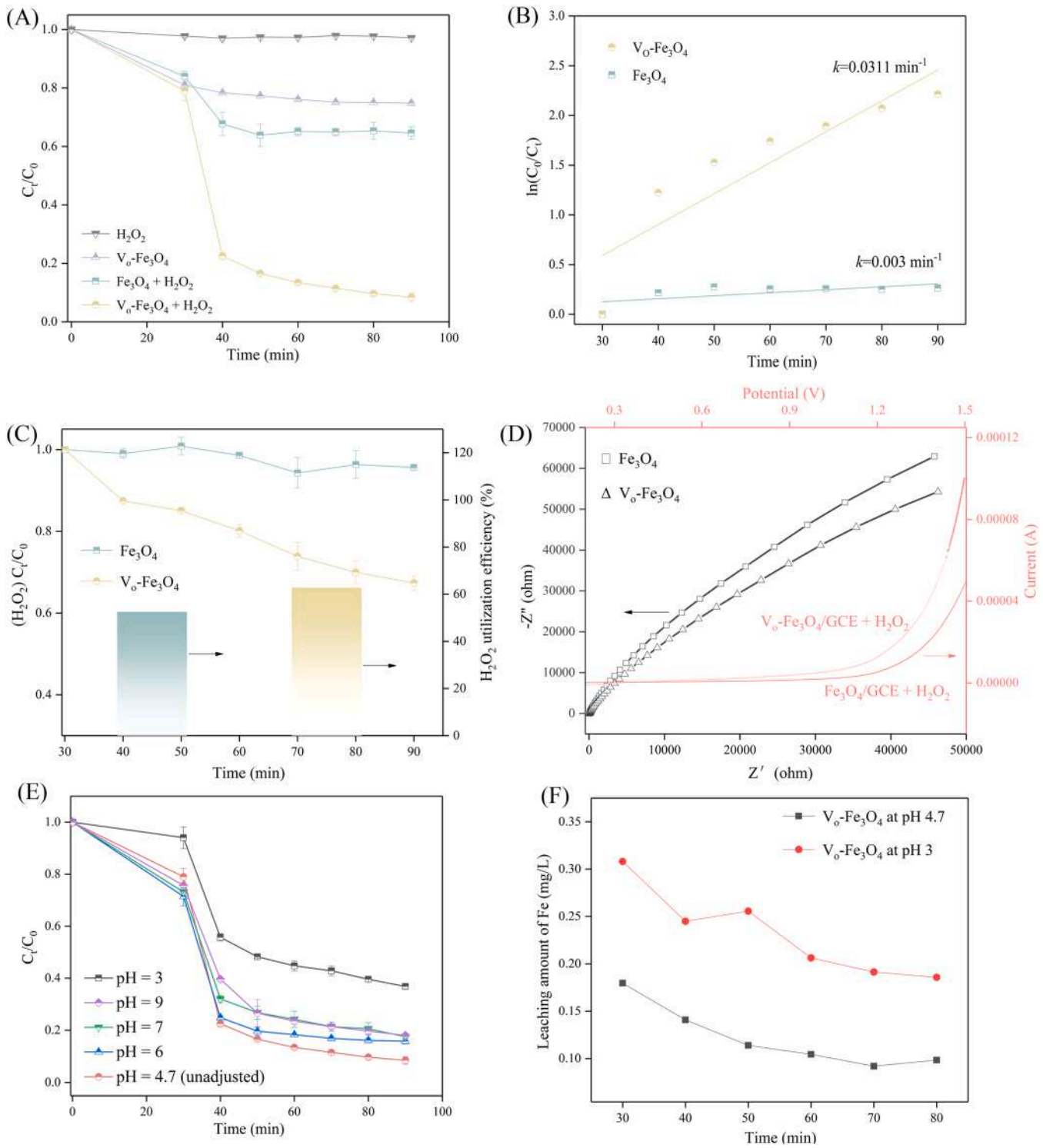

Fig. 4. (A) Degradation of OTC in different systems; (B) Corresponding pseudo-first-order kinetic of OTC degradation in different systems; (C) Decomposition of H_2O_2 by the as-prepared catalysts (left), and H_2O_2 utilization efficiency (right); (D) EIS Nyquist plots of Fe_3O_4/GCE and V_o-Fe_3O_4/GCE with frequency range from 0.01 Hz to 10^5 Hz (left), and LSV curves of Fe_3O_4/GCE and V_o-Fe_3O_4/GCE in the presence of H_2O_2 (right); (E) Effects of initial solution pH on the degradation efficiency of OTC; and (F) Leaching amount of Fe during catalytic reaction. Experimental conditions: OTC concentration= 10 mg/L; catalyst dosage= 50 mg/L; H_2O_2 concentration= 2 mmol/L;.

rate increased from 84.3% to 91.6% when H_2O_2 dosage increased from 0.5 mmol/L to 2 mmol/L (Fig. S4). While OTC degradation efficacy decreased to 87.5% and 86.9% respectively with H_2O_2 dosage further increasing to 5 mmol/L and 10 mmol/L. This may be because excessive H_2O_2 would compete with OTC to react with generated reactive species such as $^{\bullet}OH$ [25,48], then leading to the decrease of OTC degradation efficiency. Therefore, 2 mmol/L of H_2O_2 was utilized in the subsequent experiment. Besides, it is worth mentioning that compared with other works relating to Fe_3O_4-based Fenton-like process (Table S1), OTC can be effectively degraded by using less catalyst dosage (50 mg/L) and H_2O_2 dosage (2 mmol/L) in this V_o-Fe_3O_4/H_2O_2 system, suggesting that V_o-Fe_3O_4 is an effective catalyst for heterogeneous Fenton-like reaction.

Meanwhile, solution pH is an important factor affecting the Fenton-like activity. Hence, the catalytic activities of V_o-Fe_3O_4/H_2O_2 system under different initial pH (3−9) were also studied with results displayed in Fig. 4(E). It was observed that the OTC degradation efficiency at pH 3, 4.7 (unadjusted pH of OTC solution), 6, 7, and 9 was 63.2%, 91.6%, 84.3%, 82.5%, and 82.0%, respectively. In general, Fenton-like reaction is considered to be more effective under acidic condition since the generation of •OH is enhanced and •OH possesses higher oxidation potential [49]. However, a pH 3 solution resulted in a minimal degradation efficiency in this study. To explore the reason, the pH at the point of zero charge (pH_{pzc}) of V_o-Fe_3O_4 was then measured (Fig. S5). The results showed that the surface of V_o-Fe_3O_4 possessed a positive charge at pH 3. Meanwhile, according to previous studies, OTC mainly existed as H_3OTC^+ at pH 3 [50,51]. Therefore, the electrostatic repulsion would occur between OTC and Vo-Fe_3O_4 at pH 3, as confirmed by the reduced adsorption of OTC over V_o-Fe_3O_4 surface (Fig. 4(E)), which could be responsible for the decreased degradation efficiency. Furthermore, the leaching amount of Fe at pH 3 was obviously higher than that at pH 4.7 (Fig. 4(F)). The higher loss of Fe would lead to the destruction of original surface properties of V_o-Fe_3O_4, which may also be responsible for the decreased OTC degradation efficiency at pH 3 [18,25]. Besides, the variation of pH during the reaction was investigated. It was found that the solution pH changed from 4.7, 6, 7, and 9–4.72, 5.16, 6.44, and 6.76 respectively after adsorption, and there was little change in the subsequent degradation process (Fig. S6). The stable pH environment may be responsible for the good activity of V_o-Fe_3O_4/H_2O_2 system under a wide pH range (pH = 4.7–9).

In addition, the influence of some inorganic anions involving NO_3^-, Cl^-, SO_4^{2-}, as well as HCO_3^- on the catalytic activity of V_o-Fe_3O_4/H_2O_2 system were studied, since these anions usually exist in the natural waters, and can compete with target pollutant to react with •OH or $O_2^{\bullet-}$. As displayed in Fig. S7, the order in which these anions affected Fenton-like activity of V_o-Fe_3O_4 was $HCO_3^- > SO_4^{2-} > NO_3^- \approx Cl^-$. The detailed discussion is presented in Text S3. Meanwhile, this V_o-Fe_3O_4/H_2O_2 system could also remove most of OTC in natural water. The OTC degradation efficiency in lake water and river water was determined to be 81.6% and 78.2%, respectively (Fig. S8).

3.3. Reactive species analysis

Firstly, the main reactive species in Fe_3O_4/H_2O_2 system and V_o-Fe_3O_4/H_2O_2 system were semi-quantitatively estimated through EPR technology. The evident signals of DMPO-$O_2^{\bullet-}$, TEMP-$^1O_2$, and DMPO-•OH were detected (Fig. 5(A-C)), suggesting the production of $O_2^{\bullet-}$, $^1O_2$, and •OH in the above catalytic system. Meanwhile, the intensities of DMPO-$O_2^{\bullet-}$ and TEMP-$^1O_2$ in V_o-Fe_3O_4/H_2O_2 system were much stronger than that in Fe_3O_4/H_2O_2 system, indicating the higher concentration of $O_2^{\bullet-}$ and $^1O_2$ in V_o-Fe_3O_4/H_2O_2 system. The enhanced generation of $O_2^{\bullet-}$ may be because the introduction of OVs promoted the activation of DO. This hypothesis was confirmed by the Fenton-like activity of Fe_3O_4 and V_o-Fe_3O_4 under Ar atmosphere. As displayed in Fig. S9, the Fenton-like activity of Fe_3O_4 slightly altered while that of V_o-Fe_3O_4 obviously decreased under Ar atmosphere, which demonstrated the important role of DO activation in V_o-Fe_3O_4/H_2O_2 system. As for $^1O_2$, it can be found from Fig. S10 that the consumption of DPBF was obviously inhibited when TEMPOL was presented, indicating that $O_2^{\bullet-}$ was the precursor of $^1O_2$ (Eqs. (1–2)). In addition, since the reduction of Fe(III) (Fe(III)/Fe(II)) could be accelerated with the assistance of OVs, the quenching of $O_2^{\bullet-}$ by Fe(III) ($k_{Fe(III),\ O2\bullet-} = 5 \times 10^7\ M^{-1}\ s^{-1}$) [52] in V_o-Fe_3O_4/H_2O_2 system would be decreased, which consequently reduced the consumption of $O_2^{\bullet-}$. The enhanced generation and reduced consumption of $O_2^{\bullet-}$ facilitated Eqs. (1–2), and thus promoting the generation of $^1O_2$.

Nevertheless, the intensity of DMPO-•OH in V_o-Fe_3O_4/H_2O_2 system was only slightly higher than that in Fe_3O_4/H_2O_2 system. To further compare •OH generation within Fe_3O_4/H_2O_2 system and V_o-Fe_3O_4/H_2O_2 system, •OH concentration in reaction system was quantified by using BA as a probe. As seen from Fig. 5(D), •OH concentration in V_o-Fe_3O_4/H_2O_2 system was approximately 3.5 times than that in Fe_3O_4/H_2O_2 system. In this case, it was considered that the introduction of OVs significantly promoted •OH generation. Besides, the enhanced

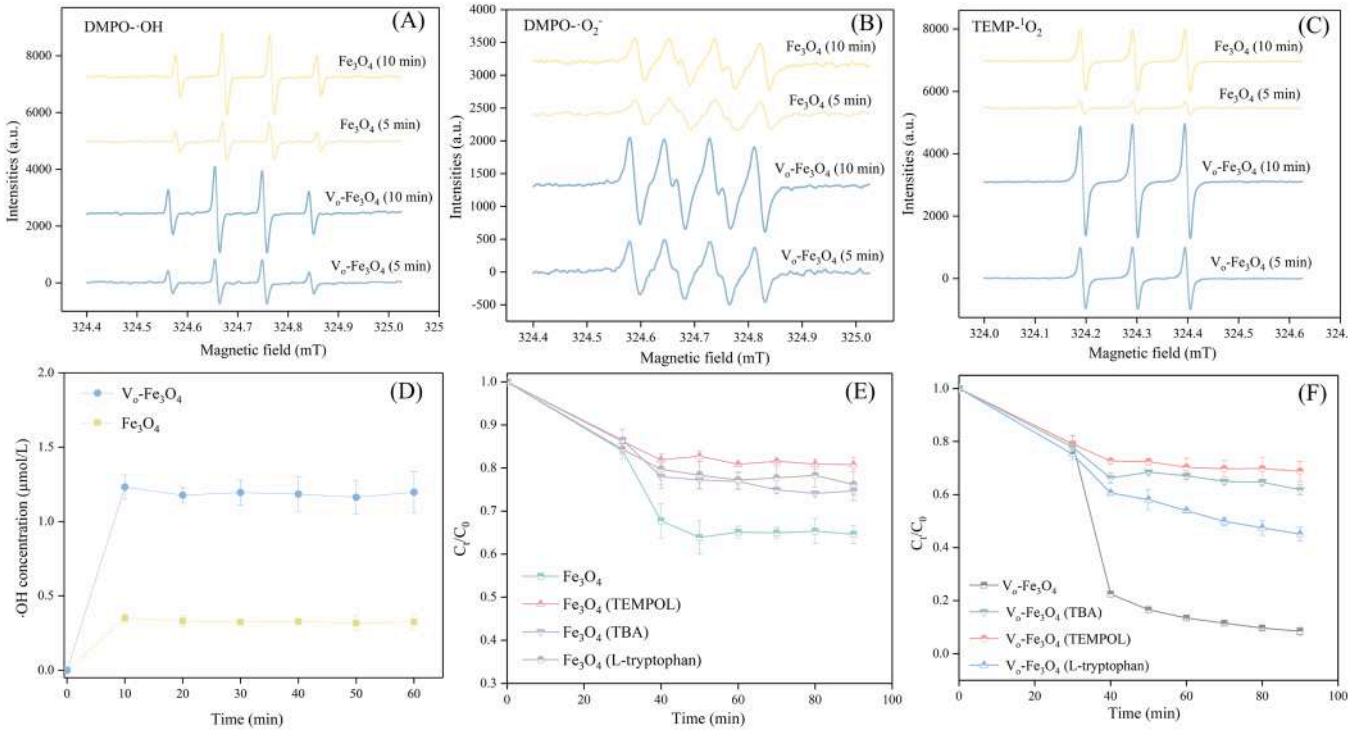

Fig. 5. (A) The EPR spectra of DMPO-•OH, (B) DMPO-$O_2^{\bullet-}$ and (C) TEMP-$^1O_2$ in Fe_3O_4/H_2O_2 system and V_o-Fe_3O_4/H_2O_2 system; (D) •OH generation in Fe_3O_4/H_2O_2 system and V_o-Fe_3O_4/H_2O_2 system; (E) The degradation curve of OTC with different inhibitors in Fe_3O_4/H_2O_2 system; and (F) The degradation curve of OTC with different inhibitors in V_o-Fe_3O_4/H_2O_2 system. Experimental conditions: OTC concentration = 10 mg/L; catalyst dosage = 50 mg/L, H_2O_2 concentration = 2 mmol/L.

generation of •OH may be related to the accelerated regeneration of Fe (II) and distinguishing electron transfer process, which will be discussed in the later section.

$$O_2^- + HO_2\cdot + H^+ \rightarrow {}^1O_2 + H_2O_2 \quad (1)$$

$$2\cdot O_2^- + 2H_2O \rightarrow {}^1O_2 + H_2O_2 + 2OH^- \quad (2)$$

Then, the role of different reactive species was studied through quenching experiments. To be specific, TBA was utilized as the quencher of •OH, TEMPOL was employed to scavenge $O_2^{\bullet-}$, and L-tryptophan was used to quench $^1O_2$. As shown in Fig. 5(E), the existence of TBA, TEMPOL, and L-tryptophan in Fe_3O_4/H_2O_2 system decreased OTC degradation efficiency to 25.3%, 16.1% and 23.9%, respectively. These results suggested that all •OH, $O_2^{\bullet-}$, and $^1O_2$ contributed to OTC degradation in Fe_3O_4/H_2O_2 system, which was in accordance with EPR results. Meanwhile, in V_o-Fe_3O_4/H_2O_2 system, the degradation efficiency of OTC decreased to 36.9%, 27.3%, and 54.9% respectively when adding TBA, TEMPOL, and L-tryptophan as quencher (Fig. 5(F)). It was found that in both Fe_3O_4/H_2O_2 system and V_o-Fe_3O_4/H_2O_2 system, $O_2^{\bullet-}$ played a major role in OTC degradation. This might because the recombination of $O_2^{\bullet-}$ and $HO_2\bullet$ was mainly responsible for $^1O_2$ generation. Therefore, the scavenger of $O_2^{\bullet-}$ could also result in the decrease of $^1O_2$, further causing a decrease in OTC degradation efficiency. Besides, in Fig. 5(E-F), the concentration of OTC appeared to increase with the degradation progressing. This may be because the adsorption-desorption process still existed when OTC could not be further degraded, which therefore resulted in a slight change in the OTC concentration in solution.

3.4. Mechanisms analysis for the V_o-Fe_3O_4 mediated Fenton-like reaction

The Fe 2p and O 1 s XPS spectra of V_o-Fe_3O_4 after reaction were analyzed to explore the activation mechanism. The results showed that the ratio of Fe(II) to Fe(III) decreased from 0.492 to 0.465 after catalytic reaction (Fig. S11(A)), which suggested the oxidation of Fe(II) to Fe(III) during activation process. Meanwhile, the OVs content of V_o-Fe_3O_4 slightly declined after reaction (Fig. S11(B)), indicating that OVs also participated in the Fenton-like process [53].

In order to further investigate the catalytic reaction between H_2O_2 and Fe_3O_4 as well as V_o-Fe_3O_4, the adsorption and charge transfer of H_2O_2 on Fe_3O_4 and V_o-Fe_3O_4 were studied through DFT calculation (Fig. 6). Firstly, the adsorption of H_2O_2 molecule on different sites of Fe_3O_4 (Fe site) and V_o-Fe_3O_4 (OVs site and Fe site adjacent to OVs) were revealed. It was calculated that the adsorption energy ($E_{(ad)}$) of H_2O_2 on Fe site of Fe_3O_4 was − 3.495 eV, and that of H_2O_2 on OVs site and Fe site adjacent to OVs was − 3.965 eV and − 3.850 eV, respectively. The most negative $E_{(ad)}$ of H_2O_2 on OVs site indicated that the adsorption of H_2O_2 on this site was the most stable. Meanwhile, the calculated charge transfer values of H_2O_2 on Fe site of Fe_3O_4, OVs site and Fe site adjacent to OVs of V_o-Fe_3O_4 were − 1.125e, 0.489e, and − 0.024e, respectively. This suggested that H_2O_2 tended to lose electrons on Fe site of Fe_3O_4 and gain electrons on OVs site of V_o-Fe_3O_4, which may be because the localized electrons of OVs assisted in donating electrons to H_2O_2, therefore benefitting the generation of •OH.

On the basis of above discussions, Fig. 6(G) proposes the possible reaction mechanism in V_o-Fe_3O_4/H_2O_2 system. Firstly, the flower-like

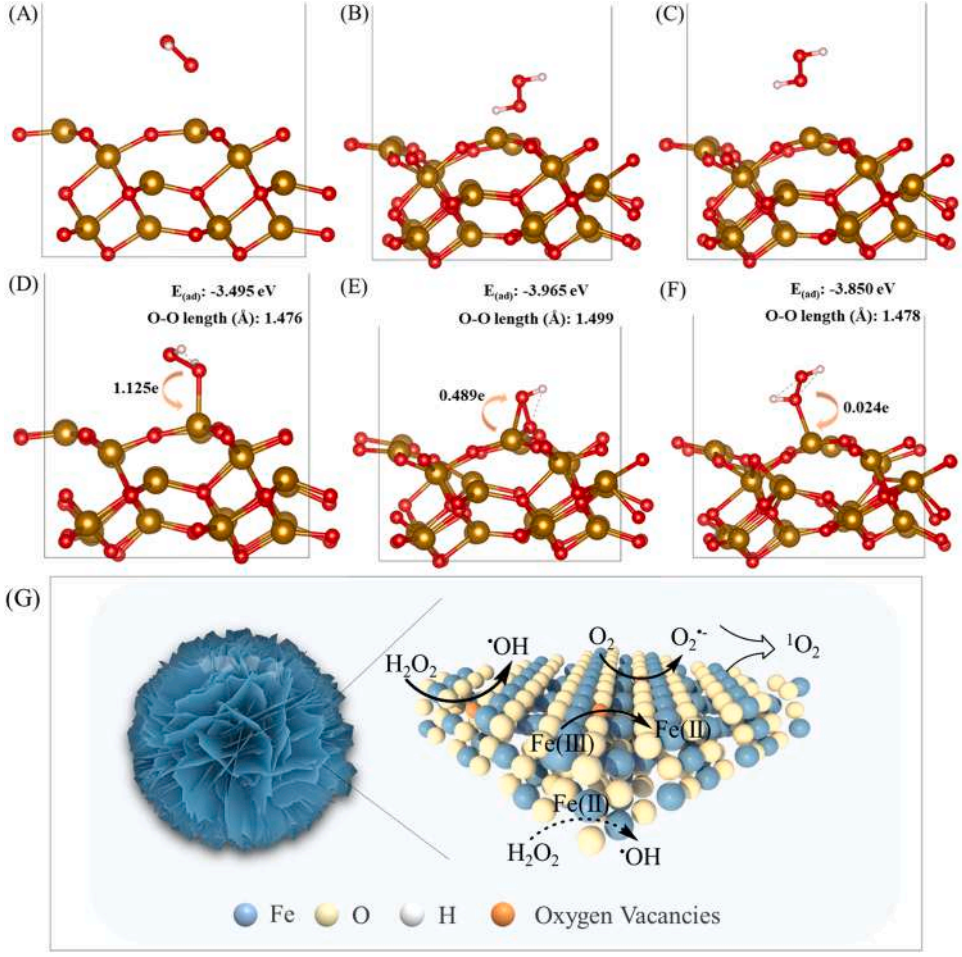

Fig. 6. Initial geometry of absorption structure of H_2O_2 on (A) Fe site of Fe_3O_4, (B) OVs site, and (C) Fe site adjacent to OVs of V_o-Fe_3O_4; Optimized geometry of absorption structure of H_2O_2 on (D) Fe site of Fe_3O_4, (E) OVs site, and (F) Fe site adjacent to OVs of V_o-Fe_3O_4; and (G) Proposed mechanism in V_o-Fe_3O_4/H_2O_2 system.

nanostructure of V_o-Fe_3O_4 enabled the exposure of abundant active sites for H_2O_2 activation. The existed Fe(II) and Fe(III) would react with H_2O_2 to generate $^{\bullet}OH$ and $HO_2^{\bullet}$ respectively through Eq. (3) and Eq (4), the unstable $HO_2^{\bullet}$ then quickly transferred to $O_2^{\bullet-}$ via Eq. (5). Besides, the Fe (III)/Fe(II) redox could be proceeded with the aid of OVs, further accelerating the catalytic reaction. Moreover, the localized electrons from OVs of V_o-Fe_3O_4 could assist in donating electrons to H_2O_2 adsorbed on OVs site, which could therefore benefit the production of $^{\bullet}OH$. Additionally, the existence of OVs promoted the activation of DO and thus the generation of $O_2^{\bullet-}$, which was possible to recombine with $HO_2^{\bullet}$ (Eq. 1) or itself (Eq. 2) to produce $^1O_2$. The generated reactive radicals then attacked OTC and its intermediates, leading to their degradation.

$$Fe(II) + H_2O_2 \rightarrow Fe(III) + \bullet OH + OH^- \quad (3)$$

$$Fe(III) + H_2O_2 \rightarrow Fe(II) + HO_2\bullet + H^+ \quad (4)$$

$$HO_2\bullet \rightleftharpoons O_2^{\bullet-} + H^+ \quad (5)$$

3.5. Identification of intermediates and toxicity analysis

LC-MS was utilized for detecting the degradation intermediates of

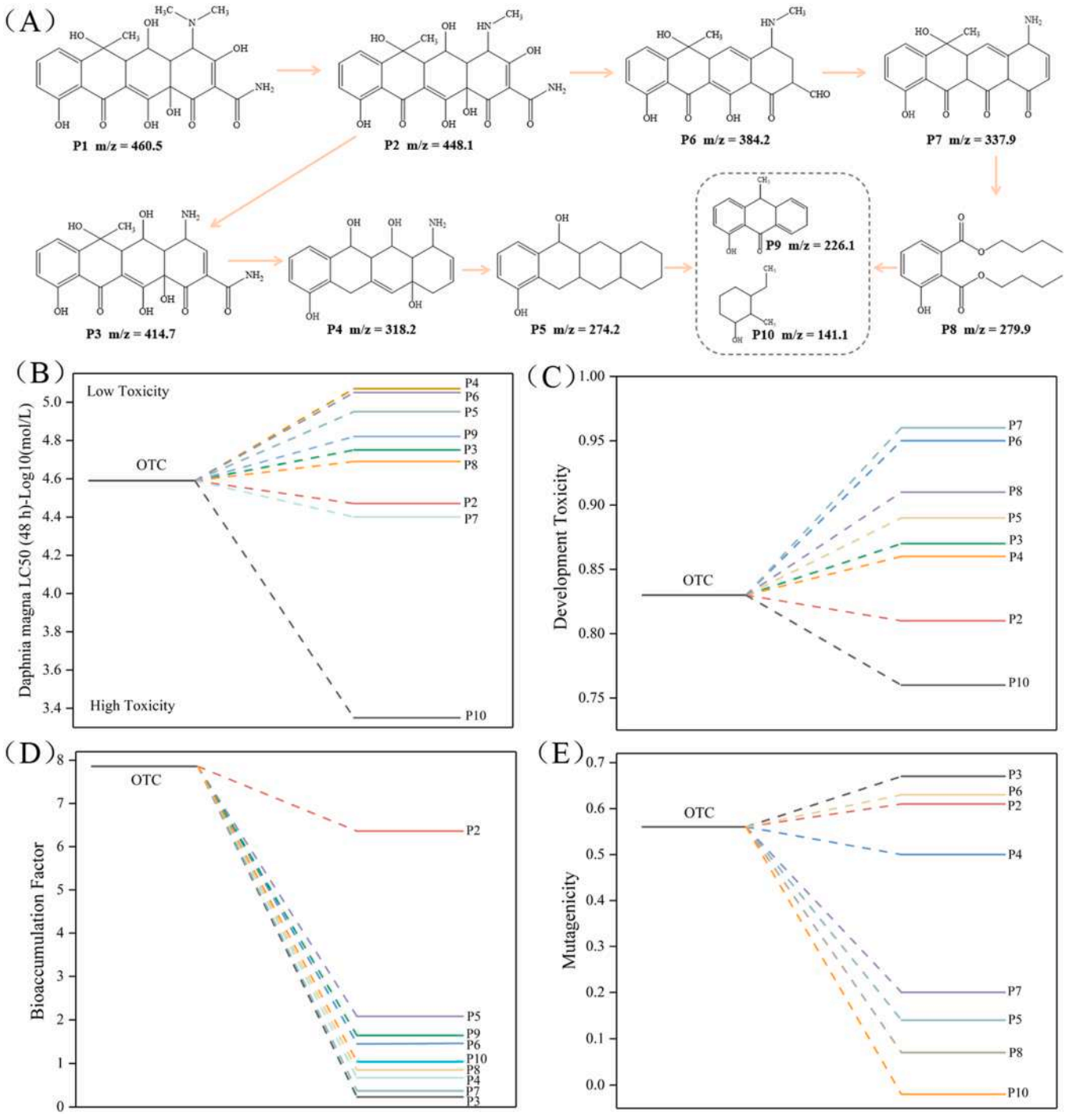

Fig. 7. (A) Possible degradation pathway of OTC in V_o-Fe_3O_4/H_2O_2 system; (B) Daphnia magna LC50 (48 h); (C) Developmental toxicity; (D) Bioaccumulation factor and (E) Mutagenicity of OTC and degradation intermediates.

OTC, and the detailed spectra are presented in Fig. S12. Based on this and relevant literature, possible OTC degradation pathways in V_o-Fe_3O_4/H_2O_2 system were then proposed (Fig. 7(A)), and the corresponding discussion is made in Text S4. Meanwhile, the possible toxicity of OTC and these intermediates were estimated through toxicity estimation software tool (T. E. S. T) [54,55]. To be specific, the Daphnia magna LC50 (48 h), development toxicity, bioconcentration factor, and mutagenicity were studied. As shown in Fig. 7(B), all intermediates except for P2, P7, and P10 showed lower Daphnia magna LC50 than OTC, indicating the reduced toxicity of these intermediates. For development toxicity (Fig. 7(C)), although some preliminary intermediates showed increased toxicity, the toxicity of P2 and P10 eventually decreased with the degradation process proceeding. Additionally, all intermediates exhibited much lower bioconcentration factor than OTC (Fig. 7(D)), clarifying their weaker ecological enrichment effects [54]. Meanwhile, the mutagenicity of most intermediates (except for P2, P3, and P6) were less negative than that of OTC (Fig. 7(E)). The above results demonstrated that not all generated intermediates showed reduced toxicity compared to OTC. Therefore, the potential environmental risks of generated intermediates are still of concern.

3.6. Investigating the long-term application of V_o-Fe_3O_4

In this study, the long-term Fenton-like performance of V_o-Fe_3O_4 was also evaluated through a continuous flow experiment in the fixed-bed reactor. It can be observed from Fig. 8(A), the pollutant water solution was passed through the catalyst packed bed by using a peristaltic pump at a flow rate of 4 mL/min, and then collected at the other end. For studying the adsorption capacity of this fixed-bed reaction for OTC, the pollutant water solution only contained 10 mg/L OTC. The result (Fig. 8 (B)) indicated that the adsorption amount decreased gradually with increase of time, and the adsorption-desorption equilibrium between catalyst packed bed and OTC was obtained at 360 min. Then, the degradation efficiency of OTC during continuous experiment was studied by using pollutant water solution containing both 10 mg/L OTC and 2 mmol/L H_2O_2. As shown in Fig. 8(C), the value of C_t/C_0 was slowly increasing and stayed below 20% within 120 h, which in turn indicated that the removal efficiency of OTC was slowly decreasing but stayed above 80% within 120 h. This result suggested the efficient removal of OTC in this fixed-bed Fenton-like reactor and proved the applicability of V_o-Fe_3O_4 in continuous experiment. Meanwhile, the ability of this V_o-Fe_3O_4/H_2O_2 system to remove COD from real wastewater was also studied. The wastewater was collected from rotational flow grit chamber of Kaifu Waste-water Treatment Plant in Changsha, Hunan province, China, and the COD was measured to be 80 mg/L. As shown in Fig. 8(D), the C_t/C_0 of COD in the effluent ranged from 50% to 78.7% within the running period, and the removal efficiency was determined to be 21.3–50%.

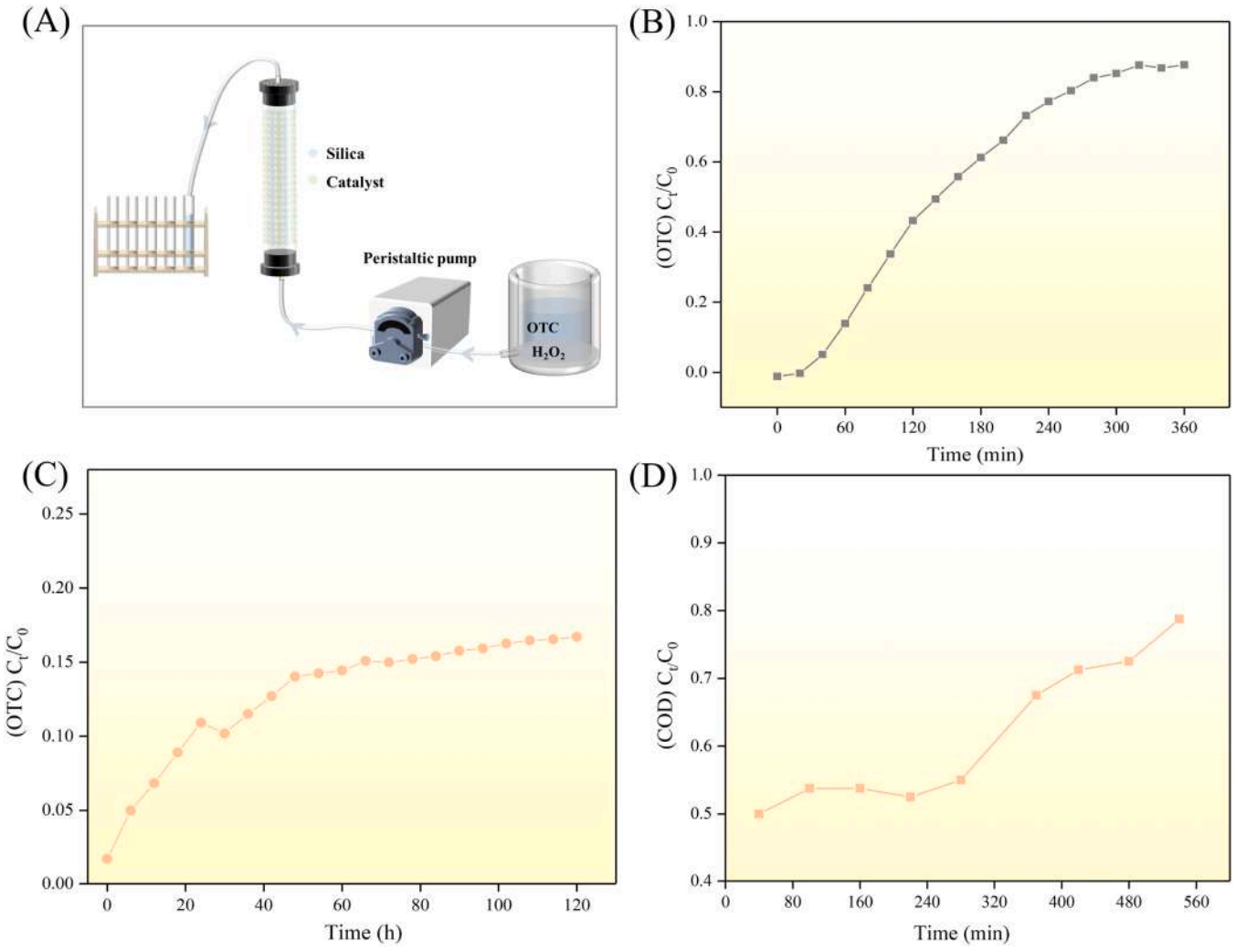

Fig. 8. (A) Schematic diagram of the continuous flow fixed-bed reactor; (B) Adsorption of OTC by the continuous flow fixed-bed reactor; (C) The removal performance of OTC by the continuous flow fixed-bed reactor; and (D) The removal performance of COD by the continuous flow fixed-bed reactor.

4. Conclusion

In summary, through a facile $NaBH_4$ reduction method, flower-like Fe_3O_4 with abundant OVs (V_o-Fe_3O_4) was successfully built, which could effectively remove OTC at a low H_2O_2 dosage with the degradation efficiency to be 91.6% and H_2O_2 utilization efficiency to be 62.8%, much higher than that of Fe_3O_4 (H_2O_2 utilization efficiency of 52.5% and OTC degradation efficiency of 35.4%). Characterization analysis, experimental results, and theoretical calculations revealed that the presence of OVs not only promoted electron transfer process, but also assisted in donating electrons to H_2O_2 and DO adsorbed on OVs site. Meanwhile, the flower-like structure facilitated the exposure of reactive sites for OTC and H_2O_2 contact, all of which contributed to the improved Fenton-like catalytic performance. In addition, the obtained V_o-Fe_3O_4 also exhibited well catalytic activity in continuous fixed-bed Fenton-like reactor. The proposed strategy in this work to enhance the H_2O_2 utilization efficiency of Fe_3O_4 provides a reference to develop scalable, and highly efficient Fenton-like catalysts for the remediation of polluted water.

Environmental Implications

How to reduce the use of chemicals doses is the key issue for application of heterogeneous Fenton-like process in wastewater remediation. In this study, magnetite (Fe3O4) with enriched oxygen vacancies (Vo-Fe3O4) was produced on a small-scale (~50 g). The prepared Vo-Fe3O4 could effectively degrade oxytetracycline (91.6%) at a low catalyst dosage (50 mg/L) and H2O2 dosage (2 mmol/L). Remarkably, further integration of Vo-Fe3O4 into fixed-bed Fenton-like reactor could effectively eliminate chemical oxygen demand (COD) (21.3%~50%) within the running period. This work provides worthy guidance for enhancing Fenton-like performance of Fe mineral toward sustainable environmental remediation.

CRediT authorship contribution statement

Ling Li: Investigation, Writing – original draft. **Min Cheng:** Investigation, conceptualization. **Eydhah Almatrafi:** Supervision, writing-review & editing. **Lei Qin:** Resources, validation. **Shiyu Liu:** Writing-review & editing. **Huan Yi:** Resources. **Lu Yang:** Data curation. **Zhexin Chen:** Resources. **Dengsheng Ma:** Formal analysis. **Mingming Zhang:** Methodology. **Xuerong Zhou:** Supervision. **Fuhang Xu:** Validation. **Chengyun Zhou:** Software. **Lin Tang:** Methodology. **Guangming Zeng:** Funding acquisition, project administration. **Cui Lai:** Project administration.

Declaration of Competing Interest

The authors declare that they have no known competing financial interests or personal relationships that could have appeared to influence the work reported in this paper.

Data Availability

Data will be made available on request.

Acknowledgments

This study was financially supported by the Program for the National Natural Science Foundation of China (U20A20323, 52170161, 52100183), the National Program for Support of Top-Notch Young Professionals of China (2014), the Program for Changjiang Scholars and Innovative Research Team in University (IRT-13R17), Hunan Researcher Award Program (2020RC3025), the Project funded by China Postdoctoral Science Foundation (2021M700041), Postgraduate Scientific Research Innovation Project of Hunan Province (CX20220383), and the National Natural Science Foundation of Changsha (kq2202166).

Appendix A. Supporting information

Supplementary data associated with this article can be found in the online version at doi:10.1016/j.jhazmat.2023.131800.

References

[1] Xu, W., Xue, W., Huang, H., Wang, J., Zhong, C., Mei, D., 2021. Morphology controlled synthesis of α-Fe_2O_{3-x} with benzimidazole-modified Fe-MOFs for enhanced photo-Fenton-like catalysis. Appl Catal B: Environ 291, 120129. https://doi.org/10.1016/j.apcatb.2021.120129.

[2] Guo, S., Wang, H., Yang, W., Fida, H., You, L., Zhou, K., 2020. Scalable synthesis of Ca-doped α-Fe_2O_3 with abundant oxygen vacancies for enhanced degradation of organic pollutants through peroxymonosulfate activation. Appl Catal B: Environ 262, 118250. https://doi.org/10.1016/j.apcatb.2019.118250.

[3] Li, L., Yin, Z., Cheng, M., Qin, L., Liu, S., Yi, H., Zhang, M., Fu, Y., Yang, X., Zhou, X., Zeng, G., Lai, C., 2023. Insights into reactive species generation and organics selective degradation in Fe-based heterogeneous Fenton-like systems: a critical review. Chem Eng J 454, 140126. https://doi.org/10.1016/j.cej.2022.140126.

[4] Liu, Y., Chen, Y., Da, Y., Xie, F., Wang, J., 2022. Advanced treatment of landfill leachate using integrated coagulation/ photo-Fenton process through in-situ generated nascent Al^{3+} and H_2O_2 by Cl, N co-doped aluminum-graphite composite. Appl Catal B: Environ 304, 121003. https://doi.org/10.1016/j.apcatb.2021.121003.

[5] Rahim Pouran, S., Abdul Raman, A.A., Wan Daud, W.M.A., 2014. Review on the application of modified iron oxides as heterogeneous catalysts in Fenton reactions. J Clean Prod 64, 24–35. https://doi.org/10.1016/j.jclepro.2013.09.013.

[6] Sun, H., Xie, G., He, D., Zhang, L., 2020. Ascorbic acid promoted magnetite Fenton degradation of alachlor: Mechanistic insights and kinetic modeling. Appl Catal B: Environ 267, 118383. https://doi.org/10.1016/j.apcatb.2019.118383.

[7] Yi, H., Lai, C., Huo, X., Qin, L., Fu, Y., Liu, S., Li, L., Zhang, M., Chen, M., Zeng, G., 2022. H_2O_2-free photo-Fenton system for antibiotics degradation in water via the synergism of oxygen-enriched graphitic carbon nitride polymer and nano manganese ferrite. Environ Sci Nano 9 (2), 815–826. https://doi.org/10.1039/D1EN00869B.

[8] Nie, M., Li, Y., He, J., Xie, C., Wu, Z., Sun, B., Zhang, K., Kong, L., Liu, J., 2020. Degradation of tetracycline in water using Fe_3O_4 nanospheres as Fenton-like catalysts: kinetics, mechanisms and pathways. New J Chem 44, 2847–2857. https://doi.org/10.1039/D0NJ00125B.

[9] Zhong, Y., Yu, L., Chen, Z.-F., He, H., Ye, F., Cheng, G., Zhang, Q., 2017. Microwave-assisted synthesis of Fe_3O_4 nanocrystals with predominantly exposed facets and their heterogeneous UVA/Fenton catalytic activity. ACS Appl Mater Inter 9 (34), 29203–29212. https://doi.org/10.1021/acsami.7b06925.

[10] Li, T., Chen, Y., Wang, X., Liang, J., Zhou, L., 2021. Modifying organic carbon in Fe_3O_4-loaded schwertmannite to improve heterogeneous Fenton activity through accelerating Fe(II) generation. Appl Catal B: Environ 285, 119830. https://doi.org/10.1016/j.apcatb.2020.119830.

[11] Do, Q.C., Kim, D.-G., Ko, S.-O., 2019. Controlled formation of magnetic yolk-shell structures with enhanced catalytic activity for removal of acetaminophen in a heterogeneous fenton-like system. Environ Res 171, 92–100. https://doi.org/10.1016/j.envres.2019.01.019.

[12] Yin, Y., Ren, Y., Lu, J., Zhang, W., Shan, C., Hua, M., Lv, L., Pan, B., 2021. The nature and catalytic reactivity of UiO-66 supported Fe_3O_4 nanoparticles provide new insights into Fe-Zr dual active centers in Fenton-like reactions. Appl Catal B: Environ 286, 119943. https://doi.org/10.1016/j.apcatb.2021.119943.

[13] Wang, S., Long, J., Jiang, T., Shao, L., Li, D., Xie, X., Xu, F., 2021. Magnetic Fe_3O_4/CeO_2/g-C_3N_4 composites with a visible-light response as a high efficiency Fenton photocatalyst to synergistically degrade tetracycline. Sep Purif Technol 278, 119609. https://doi.org/10.1016/j.seppur.2021.119609.

[14] Li, S., Cui, J., Wu, X., Zhang, X., Hu, Q., Hou, X., 2019. Rapid in situ microwave synthesis of Fe_3O_4@MIL-100(Fe) for aqueous diclofenac sodium removal through integrated adsorption and photodegradation. J Hazard Mater 373, 408–416. https://doi.org/10.1016/j.jhazmat.2019.03.102.

[15] Li, L., Yin, Z., Cheng, M., Qin, L., Liu, S., Yi, H., Zhang, M., Fu, Y., Yang, L., Tang, C., Zhou, X., Xu, F., Zeng, G., Lai, C., 2022. A potential link between the structure of iron catalysts and Fenton-like performance: from fundamental understanding to engineering design. J Mater Chem A 10 (24), 12788–12804. https://doi.org/10.1039/D2TA01860H.

[16] Lai, C., Yang, L., Li, L., Ma, D., Cheng, M., Liu, S., Zhang, M., Yan, H., Tang, C., Chen, Z., Tang, L., 2023. Design of a highly efficient Cu-based catalyst with two functional areas: The role of Cu^0 and oxygen vacancies in Fenton-like system. Chem Eng J 464, 142420. https://doi.org/10.1016/j.cej.2023.142420.

[17] Li, Z., Yang, W., Xie, L., Li, Y., Liu, Y., Sun, Y., Bu, Y., Mi, X., Zhan, S., Hu, W., 2021. Prominent role of oxygen vacancy for superoxide radical and hydroxyl radical formation to promote electro-Fenton like reaction by W-doped CeO_2 composites. Appl Surf Sci 549, 149262. https://doi.org/10.1016/j.apsusc.2021.149262.

[18] Ding, R.-R., Li, W.-Q., He, C.-S., Wang, Y.-R., Liu, X.-C., Zhou, G.-N., Mu, Y., 2021. Oxygen vacancy on hollow sphere $CuFe_2O_4$ as an efficient Fenton-like catalysis for

organic pollutant degradation over a wide pH range. Appl Catal B: Environ 291, 120069. https://doi.org/10.1016/j.apcatb.2021.120069.
[19] Dong, X., Duan, X., Sun, Z., Zhang, X., Li, C., Yang, S., Ren, B., Zheng, S., Dionysiou, D.D., 2020. Natural illite-based ultrafine cobalt oxide with abundant oxygen-vacancies for highly efficient Fenton-like catalysis. Appl Catal B: Environ 261, 118214. https://doi.org/10.1016/j.apcatb.2019.118214.
[20] Shi, Q., Deng, S., Zheng, Y., Du, Y., Li, L., Yang, S., Zhang, G., Du, L., Wang, G., Cheng, M., Liu, Y., 2022. The application of transition metal-modified biochar in sulfate radical based advanced oxidation processes. Environ Res 212, 113340. https://doi.org/10.1016/j.envres.2022.113340.
[21] Guo, X.X., Hu, T.T., Meng, B., Sun, Y., Han, Y.-F., 2020. Catalytic degradation of anthraquinones-containing H_2O_2 production effluent over layered Co-Cu hydroxides: defects facilitating hydroxyl radicals generation. Appl Catal B: Environ 260, 118157. https://doi.org/10.1016/j.apcatb.2019.118157.
[22] Pan, K., Yang, C., Hu, J., Yang, W., Liu, B., Yang, J., Liang, S., Xiao, K., Hou, H., 2020. Oxygen vacancy mediated surface charge redistribution of Cu-substituted $LaFeO_3$ for degradation of bisphenol A by efficient decomposition of H_2O_2. J Hazard Mater 389, 122072. https://doi.org/10.1016/j.jhazmat.2020.122072.
[23] Liu, S., Lai, C., Zhou, X., Zhang, C., Chen, L., Yan, H., Qin, L., Huang, D., Ye, H., Chen, W., Li, L., Zhang, M., Tang, L., Xu, F., Ma, D., 2022. Peroxydisulfate activation by sulfur-doped ordered mesoporous carbon: Insight into the intrinsic relationship between defects and $^1O_2$ generation. Water Res 221, 118797. https://doi.org/10.1016/j.watres.2022.118797.
[24] Jin, H., Tian, X., Nie, Y., Zhou, Z., Yang, C., Li, Y., Lu, L., 2017. Oxygen vacancy promoted heterogeneous Fenton-like degradation of ofloxacin at pH 3.2-9.0 by Cu substituted magnetic Fe_3O_4@FeOOH nanocomposite. Environ Sci Technol 51 (21), 12699–12706. https://doi.org/10.1021/acs.est.7b04503.
[25] Yang, X., Lai, C., Li, L., Cheng, M., Liu, S., Yi, H., Zhang, M., Fu, Y., Xu, F., Yan, H., Liu, X., Li, B., 2022. Oxygen vacancy assisted Mn-CuO Fenton-like oxidation of ciprofloxacin: Performance, effects of pH and mechanism. Sep Purif Technol 287, 120517. https://doi.org/10.1016/j.seppur.2022.120517.
[26] Kresse, G., Joubert, D., 1999. From ultrasoft pseudopotentials to the projector augmented-wave method. Phys Rev B 59 (3), 1758–1775. https://doi.org/10.1103/PhysRevB.59.1758.
[27] Clark, S.J., Segall, M.D., Pickard, C.J., Hasnip, P.J., Probert, M.I.J., Refson, K., Payne, M.C., 2005. First principles methods using CASTEP. Z für Krist - Cryst Mater 220 (5–6), 567–570. https://doi.org/10.1524/zkri.220.5.567.65075.
[28] Hammer, B., Hansen, L.B., Nørskov, J.K., 1999. Improved adsorption energetics within density-functional theory using revised Perdew-Burke-Ernzerhof functionals. Phys Rev B 59 (11), 7413–7421. https://doi.org/10.1103/PhysRevB.59.7413.
[29] Hafner, J., 2008. Ab-initio simulations of materials using VASP: density-functional theory and beyond. J Comput Chem 29 (13), 2044–2078. https://doi.org/10.1002/jcc.21057.
[30] Perdew, J.P., Burke, K., Wang, Y., 1996. Generalized gradient approximation for the exchange-correlation hole of a many-electron system. Phys Rev B 54 (23), 16533. https://doi.org/10.1103/PhysRevB.54.16533.
[31] Wang, V., Xu, N., Liu, J.-C., Tang, G., Geng, W.-T., 2021. VASPKIT: a user-friendly interface facilitating high-throughput computing and analysis using VASP code. Comput Phys Commun 267, 108033. https://doi.org/10.1016/j.cpc.2021.108033.
[32] Momma, K., Izumi, F., 2008. VESTA: a three-dimensional visualization system for electronic and structural analysis. J Appl Crystallogr 41, 653–658. https://doi.org/10.1107/S0021889808012016.
[33] Grimme, S., Antony, J., Ehrlich, S., Krieg, H., 2010. A consistent and accurate ab initio parametrization of density functional dispersion correction (DFT-D) for the 94 elements H-Pu. J Chem Phys 132 (15), 154104. https://doi.org/10.1063/1.3382344.
[34] Jain, A., Ong, S.P., Hautier, G., Chen, W., Richards, W.D., Dacek, S., Cholia, S., Gunter, D., Skinner, D., Ceder, G., Persson, K.A., 2013. Commentary: the materials project: a materials genome approach to accelerating materials innovation. APL Mater 1 (1), 011002. https://doi.org/10.1063/1.4812323.
[35] Chen, Y., Miller, C.J., Waite, T.D., 2022. pH dependence of hydroxyl radical, ferryl, and/or ferric peroxo species generation in the heterogeneous Fenton process. Environ Sci Technol 56 (2), 1278–1288. https://doi.org/10.1021/acs.est.1c05722.
[36] Chen, N., Huang, Y., Hou, X., Ai, Z., Zhang, L., 2017. Photochemistry of hydrochar: Reactive oxygen species generation and sulfadimidine degradation. Environ Sci Technol 51 (19), 11278–11287. https://doi.org/10.1021/acs.est.7b02740.
[37] Zhong, L.S., Hu, J.S., Liang, H.P., Cao, A.M., Song, W.G., Wan, L.J., 2006. Self-assembled 3D flowerlike iron oxide nanostructures and their application in water treatment. Adv Mater 18 (18), 2426–2431. https://doi.org/10.1002/adma.200600504.
[38] Gao, Q., Zhao, A., Gan, Z., Tao, W., Li, D., Zhang, M., Guo, H., Wang, D., Sun, H., Mao, R., Liu, E., 2012. Facile fabrication and growth mechanism of 3D flower-like Fe_3O_4 nanostructures and their application as SERS substrates. CrystEngComm 14 (14), 4834–4842. https://doi.org/10.1039/C2CE25198A.
[39] Ye, K., Li, K., Lu, Y., Guo, Z., Ni, N., Liu, H., Huang, Y., Ji, H., Wang, P., 2019. An overview of advanced methods for the characterization of oxygen vacancies in materials. TrAC Trend Anal Chem 116, 102–108. https://doi.org/10.1016/j.trac.2019.05.002.
[40] Ji, D., Fan, L., Tao, L., Sun, Y., Li, M., Yang, G., Tran, T.Q., Ramakrishna, S., Guo, S., 2019. The kirkendall effect for engineering oxygen vacancy of hollow Co_3O_4 nanoparticles toward high-performance portable zinc-air batteries. Angew Chem Int Ed 58 (39), 13840–13844. https://doi.org/10.1002/anie.201908736.
[41] Lai, C., Ma, D., Yi, H., Zhang, M., Xu, F., Huo, X., Ye, H., Li, L., Yang, L., Tang, L., Yan, M., 2023. Functional partition of Fe and Ti co-doped g-C_3N_4 for photo-Fenton degradation of oxytetracycline: Performance, mechanism, and DFT study. Sep Purif Technol 306, 122546. https://doi.org/10.1016/j.seppur.2022.122546.
[42] Chen, Z., Lai, C., Qin, L., Li, L., Yang, L., Liu, S., Zhang, M., Zhou, X., Xu, F., Yan, H., Tang, C., Qian, S., Sun, Q., 2023. Synergy between graphitized biochar and goethite driving efficient H_2O_2 activation: Enhanced performance and mechanism analysis. Sep Purif Technol 314, 123516. https://doi.org/10.1016/j.seppur.2023.123516.
[43] Li, J., Wan, Y., Li, Y., Yao, G., Lai, B., 2019. Surface Fe(III)/Fe(II) cycle promoted the degradation of atrazine by peroxymonosulfate activation in the presence of hydroxylamine. Appl Catal B: Environ 256, 117782. https://doi.org/10.1016/j.apcatb.2019.117782.
[44] Li, H., Shang, H., Cao, X., Yang, Z., Ai, Z., Zhang, L., 2018. Oxygen vacancies mediated complete visible light NO oxidation via side-on bridging superoxide radicals. Environ Sci Technol 52 (15), 8659–8665. https://doi.org/10.1021/acs.est.8b01849.
[45] Zhu, K., Shi, F., Zhu, X., Yang, W., 2020. The roles of oxygen vacancies in electrocatalytic oxygen evolution reaction. Nano Energy 73, 104761. https://doi.org/10.1016/j.nanoen.2020.104761.
[46] Xu, S., Zhu, H., Cao, W., Wen, Z., Wang, J., François-Xavier, C.P., Wintgens, T., 2018. Cu-Al_2O_3-g-C_3N_4 and Cu-Al_2O_3-C-dots with dual-reaction centres for simultaneous enhancement of Fenton-like catalytic activity and selective H_2O_2 conversion to hydroxyl radicals. Appl Catal B: Environ 234, 223–233. https://doi.org/10.1016/j.apcatb.2018.04.029.
[47] Lyu, L., Zhang, L., Wang, Q., Nie, Y., Hu, C., 2015. Enhanced Fenton catalytic efficiency of γ-Cu-Al_2O_3 by σ-Cu^{2+}-ligand complexes from aromatic pollutant degradation. Environ Sci Technol 49 (14), 8639–8647. https://doi.org/10.1021/acs.est.5b00445.
[48] Zhou, X., Zeng, Z., Zeng, G., Lai, C., Xiao, R., Liu, S., Huang, D., Qin, L., Liu, X., Li, B., Yi, H., Fu, Y., Li, L., Zhang, M., Wang, Z., 2020. Insight into the mechanism of persulfate activated by bone char: Unraveling the role of functional structure of biochar. Chem Eng J 401, 126127. https://doi.org/10.1016/j.cej.2020.126127.
[49] Ye, Z., Schukraft, G.E.M., L'Hermitte, A., Xiong, Y., Brillas, E., Petit, C., Sirés, I., 2020. Mechanism and stability of an Fe-based 2D MOF during the photoelectro-Fenton treatment of organic micropollutants under UVA and visible light irradiation. Water Res 184, 115986. https://doi.org/10.1016/j.watres.2020.115986.
[50] Han, C.-H., Park, H.-D., Kim, S.-B., Yargeau, V., Choi, J.-W., Lee, S.-H., Park, J.-A., 2020. Oxidation of tetracycline and oxytetracycline for the photo-Fenton process: Their transformation products and toxicity assessment. Water Res 172, 115514. https://doi.org/10.1016/j.watres.2020.115514.
[51] Liu, Y., He, X., Duan, X., Fu, Y., Dionysiou, D.D., 2015. Photochemical degradation of oxytetracycline: Influence of pH and role of carbonate radical. Chem Eng J 276, 113–121. https://doi.org/10.1016/j.cej.2015.04.048.
[52] Wang, W., Liu, Y., Yue, Y., Wang, H., Cheng, G., Gao, C., Chen, C., Ai, Y., Chen, Z., Wang, X., 2021. The confined interlayer growth of ultrathin two-dimensional Fe_3O_4 nanosheets with enriched oxygen vacancies for peroxymonosulfate activation. ACS Catal 11 (17), 11256–11265. https://doi.org/10.1021/acscatal.1c03331.
[53] Zhang, N., Xue, C., Wang, K., Fang, Z., 2020. Efficient oxidative degradation of fluconazole by a heterogeneous Fenton process with Cu-V bimetallic catalysts. Chem Eng J 380, 122516. https://doi.org/10.1016/j.cej.2019.122516.
[54] Hong, P., Wu, Z., Yang, D., Zhang, K., He, J., Li, Y., Xie, C., Yang, W., Yang, Y., Kong, L., Liu, J., 2021. Efficient generation of singlet oxygen ($^1O_2$) by hollow amorphous Co/C composites for selective degradation of oxytetracycline via Fenton-like process. Chem Eng J 421, 129594. https://doi.org/10.1016/j.cej.2021.129594.
[55] Qin, L., Ye, H., Lai, C., Liu, S., Zhou, X., Qin, F., Ma, D., Long, B., Sun, Y., Tang, L., Yan, M., Chen, W., Chen, W., Xiang, L., 2022. Citrate-regulated synthesis of hydrotalcite-like compounds as peroxymonosulfate activator - Investigation of oxygen vacancies and degradation pathways by combining DFT. Appl Catal B: Environ 317, 121704. https://doi.org/10.1016/j.apcatb.2022.121704.